Available online at www.sciencedirect.com
SCIENCE DIRECT
Journal of Molecular Catalysis A: Chemical 245 (2006) 93–100
JOURNAL OF MOLECULAR CATALYSIS A: CHEMICAL
www.elsevier.com/locate/molcata

Toluene decomposition using a wire-plate dielectric barrier discharge reactor with manganese oxide catalyst in situ

Yu-Fang Guo [a,b], Dai-Qi Ye [a,*], Ke-Fu Chen [b], Jian-Cong He [a], Wei-Li Chen [a]

[a] College of Environmental Science and Engineering, South China University of Technology, Guangzhou 510640, PR China
[b] College of Resource Science and Paper-making Engineering, South China University of Technology, Guangzhou 510640, PR China

Received 28 June 2005; received in revised form 14 September 2005; accepted 14 September 2005
Available online 27 October 2005

Abstract

Laboratory-scale experiments were performed to evaluate the efficiency of toluene decomposition by using a wire-plate dielectric barrier discharge (DBD) reactor with manganese oxide/alumina/nickel foam catalyst in the discharge area at room temperature and atmospheric pressure. The effects of oxygen content and gas flow rate were investigated. Under the optimal oxygen content and gas flow rate conditions, the combination effect of DBD and catalyst was observed, and the catalyst before/after discharge was structurally characterized by X-ray diffraction (XRD), scanning electron microscopy (SEM), and Fourier transform-infrared spectroscopy (FT-IR). It has been found that combining DBD with catalyst in situ could improve the toluene removal efficiency, increase carbon dioxide selectivity and suppress byproducts formation. Whether the catalyst existed or not, the major products were carbon dioxide and carbon monoxide when oxygen was enough. The characterization of the catalyst suggested that DBD enhanced the dispersion of the active species, increased the stability as well as the activity of the catalyst, and strengthened the oxidation capability of the catalyst, therefore the removal of toluene was promoted.

Keywords: Dielectric barrier discharge; Catalyst; Toluene; Catalytic characterization

1. Introduction

Control of volatile organic compounds (VOCs) in the atmosphere is a major environmental problem. Toluene is one of the typical VOCs. For industrial application, toluene is primarily used in manufacturing paints, paint thinners, fingernail polish, lacquers, adhesives, rubber, and some printing and leather tanning processes. Non-thermal plasma (NTP) has been investigated intensively in many countries for the abatement of VOCs. It suggested that the plasma method had some advantages when compared with the traditional catalytic ways. DBD is a common method to create NTP in which electrical energy is used to create electrons with average kinetic energy (1–10 eV). Various articles on VOCs decomposition via DBD processing have been reported. Yamamoto and co-workers investigated different VOCs using barrier type packed-bed plasma reactors [1–3]. Khassin et al. discussed the feasibility of improving the overall performance of the catalytic methane oxidation by applying a DBD [4]. Rudolph et al. studied the concentration dependence of VOC decomposition by DBDs [5]. Lee and Chang succeeded in oxidative conversion of various VOCs (such as *p*-xylene, acetaldehyde) with DBDs [6,7]. Cal and Schluep reported that near complete benzene (>99%) was destructed effectively in DBD reactors [8].

On the other hand, NTP alone has many disadvantages, such as low energy efficiencies, poor selectivity to carbon dioxide, and byproduct formation. A new attempt to overcome these limitations is the combination of the NTP method with catalysis [9–12]. Under certain conditions, a better performance could simply be achieved by a catalytic post-treatment of the NTP effluent in a two-stage process (e.g. [13–17]). In the two-stage process, the main roles of NTP are partial conversion of reactants and formation of ozone. Ozone produced in the NTP reactor can enhance the decomposition of VOCs over the subsequent catalyst bed. But for many cases, this solution is not very effective. Real synergy effects between NTP and catalysis could be available by introducing the catalyst into the discharge zone. Some researchers applied packed-bed dielectric barrier discharge to combine plasma and catalyst [18–22]. Although it has been found that packed-bed dielectric barrier discharge

* Corresponding author. Tel.: +86 20 87111279; fax: +86 20 87111279.
E-mail address: cedqye@scut.edu.cn (D.-Q. Ye).

1381-1169/$ – see front matter © 2005 Elsevier B.V. All rights reserved.
doi:10.1016/j.molcata.2005.09.013

reactor is effective in terms of energy efficiency, carbon balance, and nanometer-sized aerosol formation, the treatment of high flow of gas as required in industrial processes needs to minimize the pressure drop in the reactor due to the presence of the pellets. However, requirements for reducing pressure drop in the catalysis-assisted plasma system have rarely been discussed. In addition, the catalytic performance in the catalysis-assisted plasma system has seldom been investigated, and the function of catalysts is unclear.

On the basis of former researches on toluene decomposition in DBD reactor [23,24], and the catalytic characterization of different catalysts for pollutants removal [25,26], a wire-plate DBD reactor with a new type of manganese oxide/alumina/nickel foam catalyst in situ was designed in this paper. Nickel foam was a special support, which was thin and porous. It could be stuck on the electrodes therefore the pressure drop could be reduced greatly. Manganese-containing catalyst was chose for the low cost, environmentally friendly and relatively highly active for the combustion of volatile organic compounds [27,28]. In addition, the manganese oxides were effective in the low temperature deep oxidation of toluene to carbon dioxide and water [29] and ozone killer [14]. Parameters including oxygen content and gas flow rate were investigated. Under the optimal oxygen content and gas flow rate conditions, the combination effect of DBD and catalyst was discussed and the catalytic mechanism was proposed.

2. Experimental

2.1. Reactor

A wire-plate DBD reactor with catalyst in situ was used in the reaction (Fig. 1). Two pieces of epoxy resin boards (200 mm × 45 mm × 0.8 mm) formed the reactor walls and acted as dielectric barriers (the dielectric constant, $\varepsilon = 3.6$). The high voltage electrode was made of stainless steel wire, 0.8 mm in diameter. The wire electrode was shaped in a spiral form in order to increase the energy density in the reaction volume. The wire-to-wire distance was 10 mm and the total wire length was 3 m. Two grounded copper net electrodes were fixed on the two sides of the middle epoxy resin board. Two pieces of the nickel foam supported catalysts (150 mm × 25 mm × 2 mm) were stuck on the grounded electrodes. The total length of the reactor was 200 mm, and the effective length was 150 mm. The gap between the high voltage electrode and the grounded electrode was 8 mm, resulting in a cross-section area for flow channel of 400 mm^2 and a reaction volume of 60 cm^3.

2.2. Catalyst

Manganese oxide/alumina/nickel foam was used as a catalyst and the mass ratio of manganese oxide/alumina/nickel foam was 50%:14%:100%. An impregnation process was followed for preparing the mixed manganese oxide/alumina/nickel foam. The commercial nickel foam support was impregnated with the sol of $Al_2O_3{\cdot}nH_2O$, then the aqueous solutions of $Mn(NO_3)_2$. After that, it was dried at 393 K for 2 h, and then calcined at 723 K for 4 h.

2.3. Catalyst characterization

XRD data were obtained with the powder method in a Rigaku diffractometer (D/max-IIIA) operated at 30 kV and 30 mA, using Cu Kα radiation. The patterns were recorded over the $10^\circ < 2\theta < 100^\circ$ range and compared to the X-ray powder files to confirm phase identities.

Scanning electron micrographs were obtained with a Jeol JSM-5910 microscope operating at acceleration voltages 20 kV.

The FT-IR spectra were recorded by using an FT-IR spectrometer (Bruker Tensor 27) at room temperature. Self-supported wafers (15 mm diameter, 15 ± 1 mg) were formed by pressing the catalyst powder scratched from the catalyst. Thirty-two scans were recorded each time.

2.4. Experimental setup

The experimental setup was shown in Fig. 2. Gas streams of O_2 (>99.99%) and N_2 (>99.999%) from gas cylinders were generated and a set of mass flow controllers were used to regulate the flow rates of feeding gases. Gaseous toluene was regulated by passing part of the nitrogen gas stream through the pure toluene liquid (>99.5%) which was kept in a water bath ($T = 25 \pm 1\,^\circ C$). High voltage power was supplied by a booster (0–250 V) cooperated with a high voltage ac transformer (50 HZ, 30 kV) in series. A digital power meter (YF9901, China) was

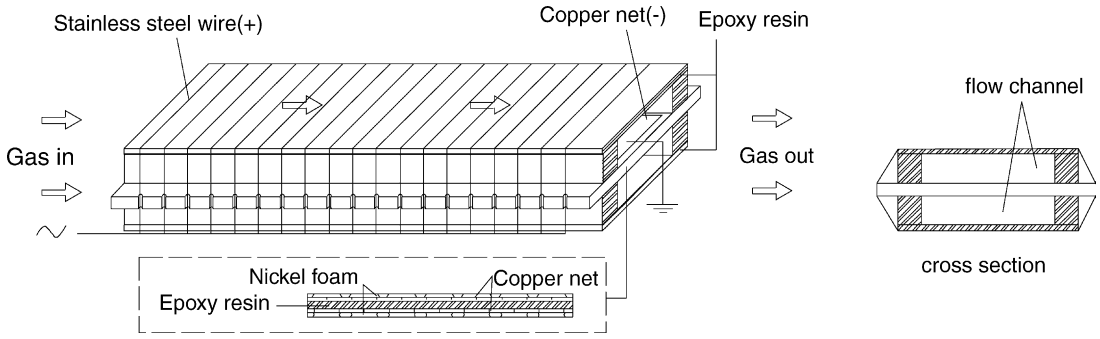

Fig. 1. Simplified structure of the DBD reactor with catalyst in situ.

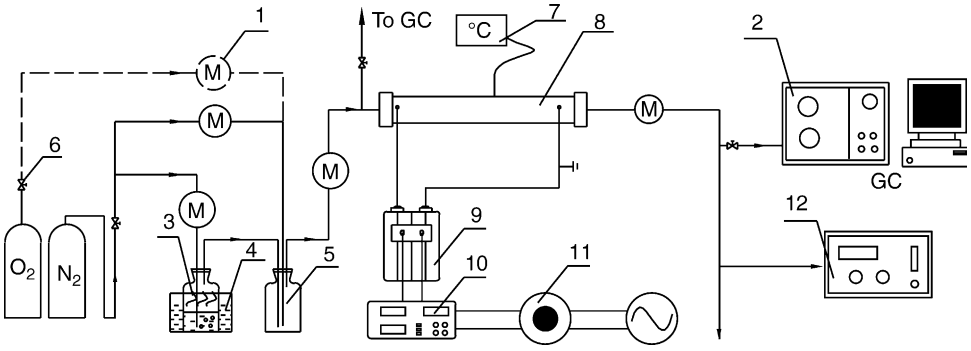

Fig. 2. Schematics of the experimental setup. *Illustration*: (1) mass flow controller, (2) gas chromatogram, (3) bubbling for toluene preparation, (4) water bath for toluene generation, (5) buffer, (6) valve, (7) temperature detector, (8) reactor, (9) ac transformer, (10) digital power meter, (11) booster, and (12) ozone analyzer.

connected to the variable voltage transformer for measuring the input power. The discharge power (the power deposited to the reactor) was calculated from the applied voltage and the reactor current. The applied voltage was measured by a high voltage probe (61010, Germany). The input power included the discharge power and power consumption on the transformer and the circuit. In this experiment, the discharge power corresponded to the input power by the factor varied from 0.5 to 0.63 in the DBD combined with catalyst system, and the factor of about 0.35 in the DBD system.

Gas samples were obtained from the effluent by an autosampler and were analyzed on-line. Toluene and the reaction products were analyzed by a gas chromatograph (GC-900A, China) equipped with two hydrogen flame ionization detectors. One was for organic compounds (such as methane, benzene and toluene) detection with a 50 m SE-30 capillary column heated at 80 °C, and the other equipped with a methanizer was for carbon monoxide and carbon dioxide analysis using a 2 m carbon molecular sieve stainless steel column heated at 65 °C. Minor products were measured by a GC–MS (HP 5973N) equipped with a 60 m DB-5MS capillary column at 40–220 °C. The ozone concentration was monitored by an ozone analyzer (DCS-1, China). The experiment was carried out at room temperature and atmospheric pressure.

The toluene removal efficiency, carbon dioxide selectivity, carbon balance value, and energy density in the gas phase were defined as follows:

Toluene removal efficiency:

$$\eta_t\,(\%) = \frac{[\text{toluene}]_{\text{inlet}} - [\text{toluene}]_{\text{exhaust}}}{[\text{toluene}]_{\text{inlet}}} \times 100\%$$

Carbon dioxide selectivity:

$$S_{CO_2}\,(\%) = \frac{[CO_2]}{[CO] + [CO_2]} \times 100\%$$

Carbon balance value:

$$\text{CB}\,(\%) = \frac{\sum C_{\text{measured}}}{\sum C_{\text{feed}}} \times 100\%$$

where $\sum C_{\text{measured}}$ is the total moles of carbon measured in the outlet stream and $\sum C_{\text{feed}}$ is the total moles of carbon fed into reactor.

Specific energy density:

$$\text{SED}\,(\text{J/l}) = \frac{\text{discharge power (W)}}{\text{gas flow rate (l/ min)}} \times 60$$

Energy efficiency:

$$\eta_E\,(\text{g/kWh}) = \frac{[\text{toluene}]_{\text{removal}} \times \text{gas flow rate}}{\text{input power}}$$

3. Results and discussion

3.1. Effect of oxygen content on toluene decomposition in the DBD combined with catalyst system

Fig. 3 shows the effect of oxygen content in the gas stream on toluene removal efficiency for selected specific energy densities in the DBD combined with catalyst system. Oxygen content varied from 0 to 20 vol%. The initial concentration of toluene was

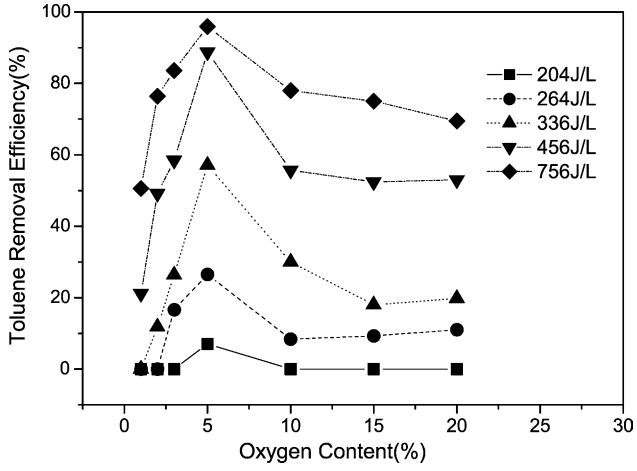

Fig. 3. Dependence of toluene removal efficiency on oxygen content for selected specific energy densities in the DBD combined with catalyst system. 50 ppmv toluene and 100 ml/min.

Table 1
Major initiating radical reactions for air discharge

Reactions		K (cm^3 $molecule^{-1}$ s^{-1})
$e + O_2 \rightarrow O_2(^1\Delta_g) + e$	(1)	7.3e−10
$e + O_2 \rightarrow O + O + e$	(2)	8.9e−10
$e + O_2(^1\Delta_g) \rightarrow O + O + e$	(3)	8.9e−10
$e + O_2 \rightarrow O + O(^1D) + e$	(4)	2.7e−09
$e + O_2(^1\Delta_g) \rightarrow O + O(^1D) + e$	(5)	2.7e−09
$O + O_2 + M \rightarrow O_3 + M$	(6)	1.4e−14
$O + O_3 \rightarrow O_2 + O_2$	(7)	8.0e−15
$e + N_2 \rightarrow e + N_2(A)$	(8)	1.4e−09
$e + N_2 \rightarrow N^* + N + e$	(9)	9.4e−11

N^* is electronically excited nitrogen species.

50 ppmv, and the gas flow rate was 100 ml/min. It was found that toluene removal efficiency increased with the increase of specific energy density, and the highest toluene removal efficiency was observed for the gas stream containing 5% oxygen. When the oxygen content was 5% and the specific energy density reached 756 J/l, the toluene removal efficiency of 95.9% was achieved.

Oxygen plays a very important role in the reaction. A low-temperature electrical discharge in an oxygen-containing gas mixture produced mainly oxygen radicals as active species. Rate constants for major initiating radical reactions involving the excitation and dissociation of O_2 and N_2 were given in Table 1 [30]. A higher oxygen content in the gas streams leads to the generation of more highly reactive O radicals in the reactor, resulting in a higher removal efficiency. However, oxygen has an adverse effect on toluene removal due to its electronegative characteristics. Increasing oxygen content would limit electron density in the system, and reduce the power deposited into the plasmas [6]. As a result, appropriate oxygen content is essential for toluene destruction.

3.2. Effect of gas flow rate on toluene decomposition in the DBD combined with catalyst system

Dependence of toluene removal efficiency on specific energy densities with the gas flow rate ranging from 100 to 500 ml/min in the combined DBD with catalyst system was shown in Fig. 4. The initial concentration of toluene was 50 ppmv, and the oxygen content was 5%. It was clear that flow rate had a significant effect on the destruction efficiency. The toluene removal efficiency increased with the decreasing of gas flow rate. Almost all toluene were destroyed at a gas flow rate of 100 ml/min under the specific energy density of 756 J/l. Decreasing the gas flow rate, namely increasing the retention time in the reactor, would cause that a molecule of the gas was submitted to an increasing number of plasma discharge and the probability of collision between toluene molecules and electrons improved, which resulted in a higher toluene removal efficiency.

3.3. Combination effect with catalyst

3.3.1. Toluene decomposition

Experimental tests were conducted to determine the dependence of toluene removal efficiency on specific energy density, energy efficiency and input power with/without catalyst (Fig. 5a–c). The optimized reaction condition of 5% O_2 and 100 ml/min was applied to the system. The initial toluene concentration was 50 ppmv. It suggested that toluene removal efficiency and energy efficiency increased significantly but the input power decreased when the specific energy density was larger than 264 J/l and manganese oxide/alumina/nickel foam catalyst was introduced into the discharge area. For example, when toluene was decomposed at 456 J/l without catalyst, toluene removal efficiency was 51.4% compared to 88.8% with catalyst, the energy efficiency of 0.67–0.29 g/kWh, and the input power of 5.76–9 kJ/h.

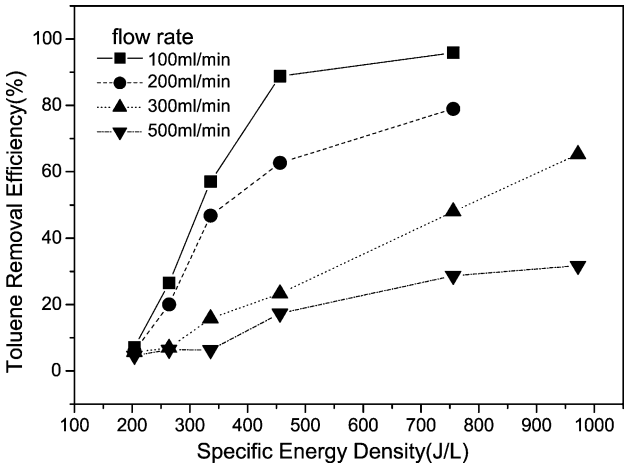

Fig. 4. Dependence of toluene removal efficiency on specific energy density for selected gas flow rates in the DBD combined with catalyst system. 50 ppmv toluene and 5% O_2.

3.3.2. Products and byproducts analysis

Products and byproducts analysis by the GC and GC–MS on different oxygen content in the DBD system without catalyst was shown in Table 2. When oxygen was enough ($1\% \leqq [O_2] \leqq 20\%$), almost all removed toluene were oxidized to carbon monoxide and carbon dioxide. And ozone was the only byproduct. Whereas some byproducts, such as CH_4, C_2H_6, $C_{12}H_{26}$, HCN were detected, and the carbon balance value was smaller than 65% when oxygen content was less than 1%. The products and byproducts composition in the DBD system with catalyst was similar to that of no catalyst in the DBD system, except for the amount of the byproducts was less. In addition, certain yellow product that was observed in the DBD reactor without catalyst did not appear in that with catalyst. The composition of the yellow products was indistinct. Maybe it was aromatic polymer.

Table 2
Products and byproducts analysis in the DBD system (50 ppmv toluene, 100 ml/min)

Oxygen content [O_2]	Products	Byproducts
$1\% \leqq [O_2] \leqq 20\%$	CO, CO_2 CB = 100 ± 2%	O_3
$[O2] \leqq 1\%$	CO, CO_2 CB < 65%	HCN, CH_4, C_2H_6, $C_{12}H_{26}$

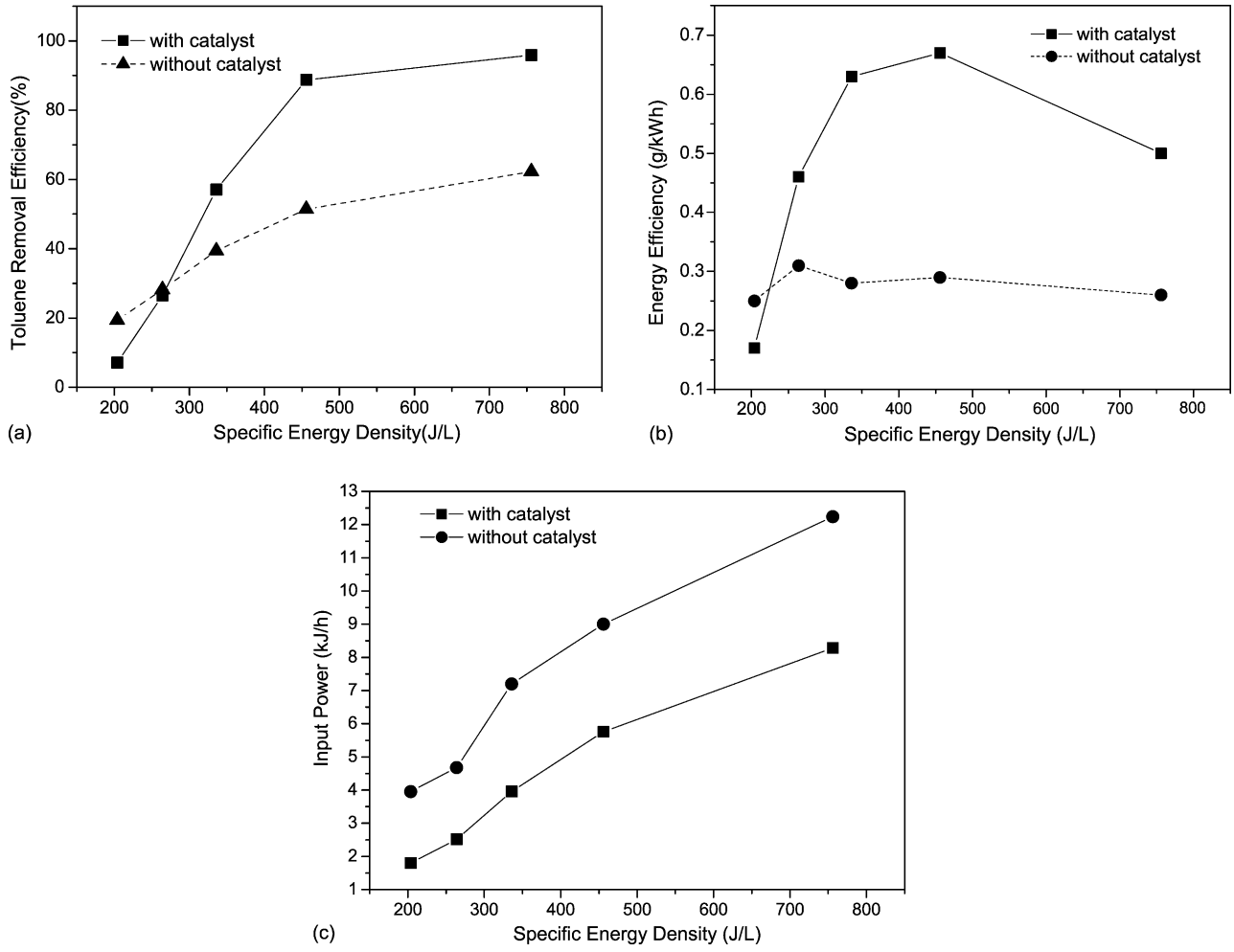

Fig. 5. Dependences of (a) toluene removal efficiency, (b) energy efficiency, and (c) input power on specific energy density in DBD reactor with/without catalyst. 50 ppmv toluene, 5% O_2, and 100 ml/min.

Decomposition of toluene via DBD could generally be achieved through three channels, i.e., (1) electron impact dissociation, (2) gas-phase radical reactions, and (3) ion–molecule reactions. Some articles reported that electron impact was the most important channel during the discharging periods and responsible for the initial reaction for toluene decomposition. Radical attack was another important mechanism leading to toluene destruction. On the other hand, toluene decomposition by direct ion process was not significant [6,31,32]. Table 3 shows the expected toluene-destruction process by non-thermal plasma

Table 3
Removal of toluene reaction by non-thermal plasma

Reactions		K (cm^3 $molecule^{-1}$ s^{-1})
$C_6H_5CH_3 + e \rightarrow$ products	(10)	e−6
$C_6H_5CH_3 + O^+, O_2^+, N, N_2^+ \rightarrow C_6H_5CH_3^+ + O, O_3, N, N_2$	(11)	e−10
$C_6H_5CH_3^+ + e \rightarrow C_6H_5 + CH_3$	(12)	e−7
$C_6H_5CH_3 + OH \rightarrow C_6H_5CH_3OH$	(13)	5.2e−12
$C_6H_5CH_3 + OH \rightarrow C_6H_5CH_2 + H_2O$	(14)	7e−13
$C_6H_5CH_3 + O \rightarrow C_6H_5CH_2O + H$	(15)	8.4e−14
$C_6H_5CH_3 + O_3 \rightarrow C_6H_5CHO_2 + H_2O$	(16)	1.5e−22

[31]. When oxygen was sufficient, almost all the hydrocarbon generated from reactions (10) to (16) would be converted to CO, CO_2, and H_2O in DBD system. But when oxygen was absent, the radicals, such as OH, O, and O_3 were not enough for complete oxidation of toluene. It led to byproducts production. Nitrogen atoms should be reckoned as a source in the formation of nitrogen-containing compounds. The catalyst could react with byproducts selectively which led to the reduction of byproducts.

The influence of the catalyst on ozone formation was presented in Fig. 6. It showed that ozone concentration increased with the increase of specific energy density, and the catalyst could reduce the ozone formation to a great extent. Ozone as the main long-living radical was transported to the catalyst and could take part in heterogeneous oxidation reactions on its surface. Futamura et al. reported the plausible mechanism for MnO_2-catalyzed decomposition of O_3 as follows [14].

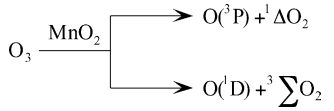

Fig. 7 shows the dependence of carbon dioxide selectivity on specific energy density with/without catalyst. From this figure, it was found that the S_{CO_2} ranged from 64 to 68% in the DBD

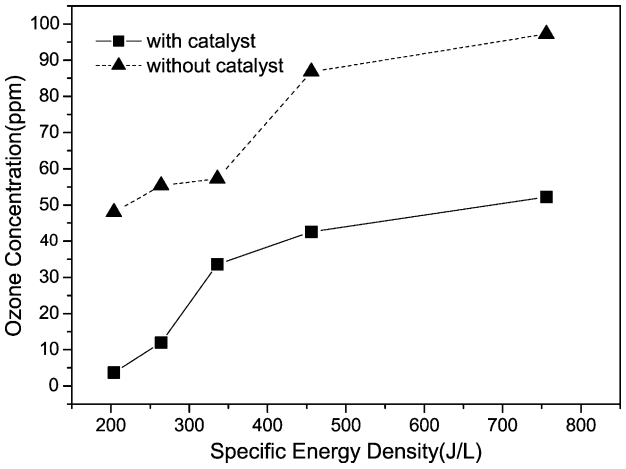

Fig. 6. Dependence of ozone concentration on specific energy density with/without catalyst. 50 ppmv toluene, 5% O_2, and 100 ml/min.

reactor without catalyst, while the S_{CO_2} ranged from 73 to 81% in the combined DBD with catalyst reactor. And the S_{CO_2} was independent of the specific energy density. The selectivity was enhanced due to the toluene oxidation near and/or on the catalyst surface.

3.4. Characterization of manganese oxide/alumina/nickel foam catalyst

The characterization of the catalyst was compared before/after discharge by XRD, SEM, and FT-IR. The catalyst was carried out after about 40 h experiments of toluene decomposition with DBD application. The specific energy density was 756 J/l, the gas streams contained 50 ppmv toluene, the oxygen content was 5% and the gas flow rate was 100 ml/min.

3.4.1. XRD spectra

Fig. 8 shows the typical XRD spectra of the manganese oxide/alumina/nickel foam catalyst before reaction. It could be seen that three characteristic components of Ni, $MnAl_2O_4$, and Mn_2O_3 (orthorhombic) were identified. The XRD spectra suggested that the catalyst loading Mn onto Al_2O_3 and nickel foam by impregnation method was a metal oxide state rather than a metallic state. Ni came from the nickel foam support. Fig. 9 shows the XRD spectra of the catalyst after discharge. It was found that the composition of Mn_2O_3 in the catalyst changed to Mn_3O_4 after discharge. The proportion of manganese oxide increased while the aluminate decreased after DBD application.

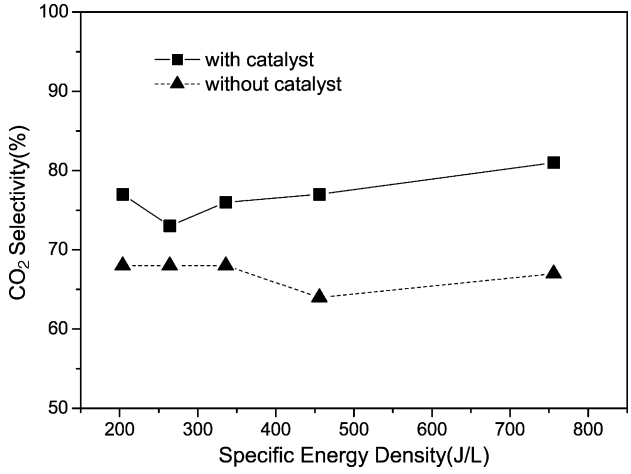

Fig. 7. Dependence of carbon dioxide selectivity on specific energy density with/without catalyst. 50 ppmv toluene, 5% O_2, and 100 ml/min.

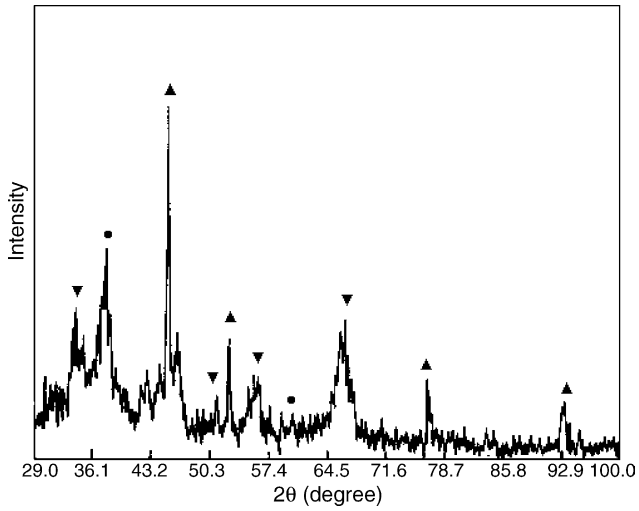

Fig. 8. XRD testing results of manganese oxide/alumina/nickel foam catalyst before reaction ((▲) Ni; (▼) Mn_2O_3 (orthorhombic); (●) $MnAl_2O_4$).

Manganese oxides are known to be active catalysts in several oxidation or reduction reactions. Manganese oxides can be used as catalysts for the oxidation of carbon monoxide [33,34] or the selective reduction of nitrobenzene [35]. Moreover, the application of manganese oxides as an oxygen storage component (OSC) for a three-way catalyst has been proposed. In all of these applications the redox properties of manganese oxides play a key role [36]. In this reaction, manganese oxides are reduced to a lower-valent manganese oxide. Once the manganese oxide is reduced, it can be regenerated, i.e. reoxidized. The oxidation

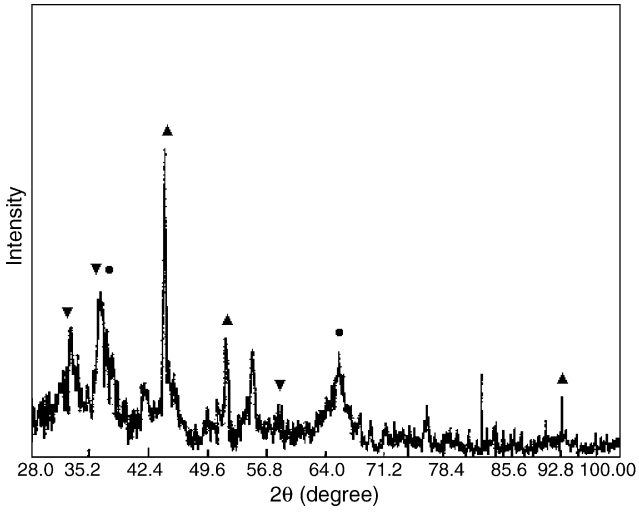

Fig. 9. XRD testing results of manganese oxide/alumina/nickel foam catalyst after DBD reaction. 756 J/l, 50 ppmv toluene, 5% O_2, and 100 ml/min ((▲) Ni; (▼) Mn_3O_4; (●) $MnAl_2O_4$).

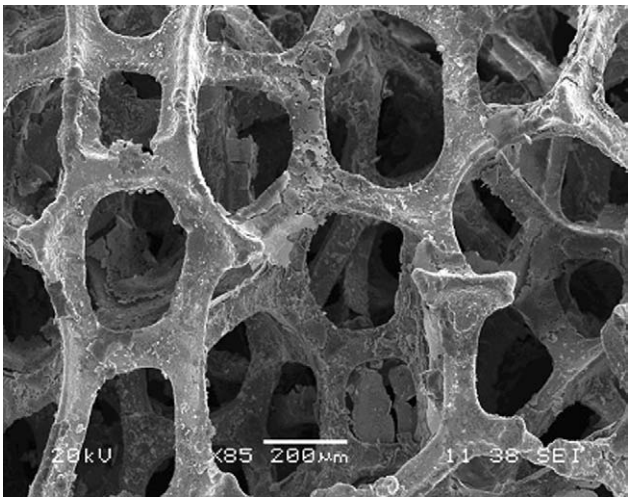

Fig. 10. The SEM image of manganese oxide/alumina/nickel foam catalyst before reaction (85×).

capability of Mn_3O_4 was better than Mn_2O_3, as a result it was in favor of enhancing the toluene oxidation. In addition, in oxidation of toluene lattice oxygen is consumed. Therefore, in principle, manganese oxides should be able to oxidize toluene even in the absence of gas-phase oxygen.

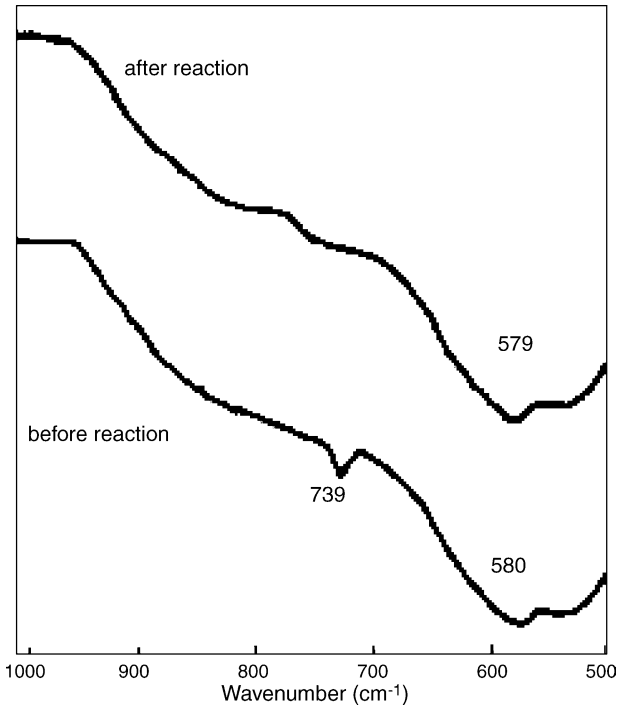

Fig. 12. Comparison of FT-IR result of manganese oxide/alumina/nickel foam before/after reaction.

3.4.2. SEM image

Fig. 10 shows the SEM images of the catalyst before reaction (magnification values of 85×). This figure illustrated that nickel foam had a pentagonal framework, and on the surface of the nickel foam there were a lot of small holes which led to a large surface area. The active component was loaded on the nickel foam with crystal form widespread over the support surface. Fig. 11 compares the SEM images of the catalyst before and after reaction ((magnification values of 1000×). It was found that the granularity of the grain on the catalyst surface became smaller and the distribution became more uniform after discharge. The ultrafine particle catalysts have large specific surface and less-perfect crystal lattice with a large number of vacancies, which induce a high catalytic activity. It proposed that DBD could enhance the dispersion of the active component, the stability as well as the catalytic activity of the catalyst in the reaction. It was reported that some unusual chemical activities had been achieved when plasma species were involved in the catalyst surface reactions, which led to efforts to apply plasmas directly to prepare more effective catalysts [37,38]. Zhang et al. demonstrated that the glow discharge treatment leads to a higher and stable dispersion of active species over the support. Also a better activity and a significantly enhanced stability of the catalysts were achieved [39]. Chen et al. found that the conversion and selectivity of the catalysts prepared by glow discharge plasma were superior to those obtained from the conventional catalysts

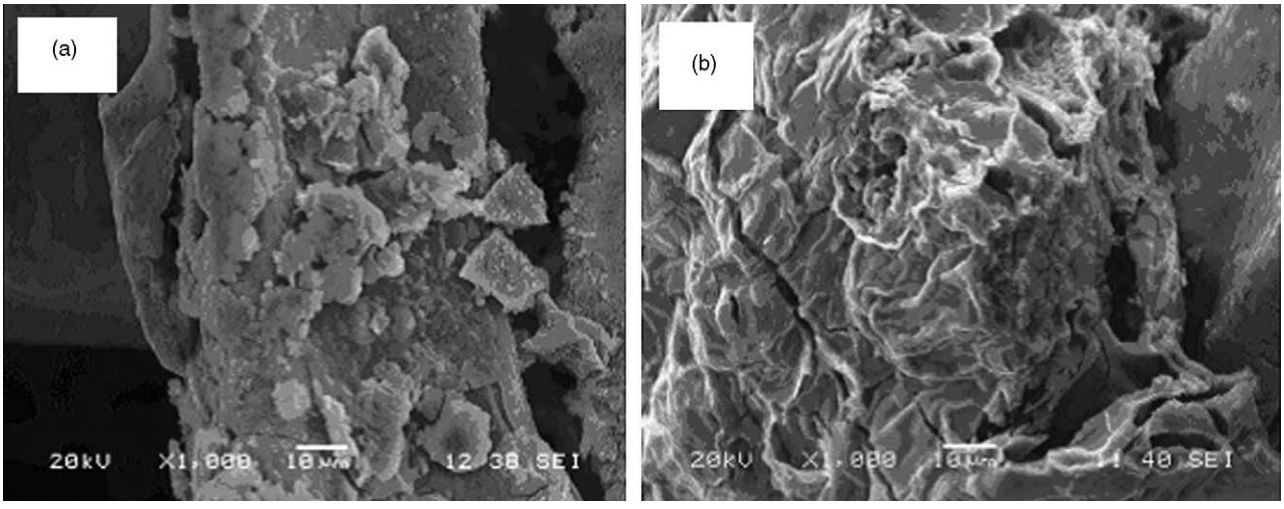

Fig. 11. Comparison of SEM images of manganese oxide/alumina/nickel foam before/after DBD reaction (1000×) (a) before reaction and (b) after DBD reaction.

[40]. The results of this reaction were in good agreement with these articles.

3.4.3. FT-IR spectra

The FT-IR spectra of catalyst before and after reaction were presented in Fig. 12. Except the absorption bands of the adsorbed water between 3000 and 3600, 1600 and1670 cm^{-1}, and the band of CO_2 at 2349 cm^{-1} in the spectra, the band of aluminate at about 750 cm^{-1} was detected in the spectra of the catalyst before reaction. The bands at 500–600 cm^{-1} corresponded to the vibration of the manganese oxide (Mn–O). The spectra of the catalyst after reaction were quite the same with those before reaction, but the transmittivity increased, which suggested that the grain of the catalyst became smaller, and highly dispersed on the support. Especially, the band of aluminate in the spectrum of the catalyst disappeared after reaction while the band of manganese oxide was sharper. It suggested that the manganese aluminate decomposed to manganese oxide under the electric field. These results were in consistent with those of the XRD and SEM.

4. Conclusions

This study demonstrated an atmospheric-pressure DBD reactor with catalyst in situ for toluene removal. The combination of dielectric barrier discharge and manganese oxide/alumina/nickel foam catalyst could improve the toluene removal efficiency and carbon dioxide selectivity, and suppress byproduct (such as ozone) formation. The potential catalytic mechanism in the combined DBD with catalyst system was proposed that the DBD could enhance the dispersion of the active species, increase the stability as well as the activity of the catalyst, strength the oxidation capability of the catalyst, consequently the removal of toluene could be promoted.

Acknowledgements

This work was partially supported by National Nature Science Foundation of China (20577011), Guangdong Province Key Scientific and Technological Project (2001367,2002254) and Guangzhou City Key Scientific and Technological Project (2001-Z-016-01).

References

[1] M. Okubo, T. Kuroki, H. Kametaka, T. Yamamoto, IEEE Trans. Ind. Appl. 2 (2000) 868.
[2] T. Yamamoto, K. Ramanathan, P.A. Lawless, D.S. Ensor, J.R. Newsome, N. Plaks, G.H. Ramsey, IEEE Trans. Ind. Appl. 28 (1992) 528.
[3] S. Futamura, T. Yamamoto, P.A. Lawless, IEEE Trans. Ind. Appl. 2 (1995) 1453.
[4] A.A. Khassin, B.L. Pietruszka, M. Heintze, V.N. Parmon, React. Kinet. Catal. Lett. 82 (2004) 131.
[5] R. Rudolph, K.-P. Francke, H. Miessner, Plasma Chem. Plasma Process. 22 (2002) 401.
[6] H.M. Lee, M.B. Chang, Plasma Chem. Plasma Process. 23 (2003) 541.
[7] H.M. Lee, M.B. Chang, Plasma Chem. Plasma Process. 21 (2001) 329.
[8] M.P. Cal, M. Schluep, Environ. Prog. 20 (2001) 151.
[9] U. Roland, F. Holzer, F.-D. Kopinke, Catal. Today 73 (2002) 315.
[10] A. Ogata, N. Shintani, K. Mizuno, S. Kushiyama, Decomposition of benzene using non-thermal plasma reactor packed with ferroelectric pellet, in: IEEE Industry Application Society Annual Meeting, New Orleans, Louisiana, October 5–9, 1997, pp. 1975–1982.
[11] C. Ayrault, J. Barrault, N. Blin-Simiand, F. Jorand, S. Pasquiers, A. Rousseau, J.M. Tatibouët, Catal. Today 89 (2004) 75.
[12] S. Futamura, H. Einaga, H. Kabashima, L.Y. Hwan, Catal. Today 89 (2004) 89.
[13] V. Demidiouk, J.O. Chae, IEEE T. Plasma Sci. 33 (2005) 157.
[14] S. Futamura, A. Zhang, H. Einaga, H. Kabashima, Catal. Today 72 (2002) 259.
[15] K.-P. Francke, H. Miessner, R. Rudolph, Plasma Chem. Plasma Process. 20 (2000) 393.
[16] V. Demidiouk, S.I. Moon, J.O. Chae, Catal. Commun. 4 (2003) 51.
[17] H. Einaga, T. Ibusuki, S. Futamura, IEEE Trans. Ind. Appl. 2 (2000) 858.
[18] A. Ogata, H. Einaga, H. Kabashima, S. Futamura, S. Kushiyama, H.-H. Kim, Appl. Catal. B: Environ. 46 (2003) 87.
[19] F. Holzer, U. Roland, F.-D. Kopinke, Appl. Catal. B: Environ. 38 (2002) 163.
[20] D. Li, D. Yakushiji, S. Kanazawa, T. Ohkubo, Y. Nomoto, J. Electrostat. 55 (2002) 311.
[21] H.-H. Kim, S.-M. Oh, A. Ogata, S. Futamura, Appl. Catal. B: Environ. 56 (2005) 213.
[22] M. Kang, B.-J. Kim, S.M. Cho1, C.-H. Chung, B.-W. Kim, G.Y. Han, K.J. Yoon, J. Mol. Catal. A: Chem. 180 (2002) 125.
[23] Y.F. Guo, D.Q. Ye, K.F. Chen, Effect of oxygen content on toluene decomposition in wire-plate dielectric barrier discharge reactor, in: Fifth Electrohydrodynamics International Workshop, Poitiers, France, August 30–31, 2004, pp. 327–331.
[24] J.C. He, R.H. Zeng, D.Q. Ye, Decomposition of Toluene by using dielectric barrier discharge reactor combined with catalysts, in: Fifth Electrohydrodynamics International Workshop, Poitiers, France, August 30–31, 2004, pp. 332–335.
[25] L.Q. Tian, D.Q. Ye, H. Liang, Catal. Today 78 (2003) 159.
[26] D.Q. Ye, M.L. Fu, L.Q. Tian, H. Liang, T.Z. Rong, S.Z. Cheng, X.S. Pang, Res. Chem. Intermed. 29 (2003) 271.
[27] W.B. Li, W.B. Chu, M. Zhuang, J. Hua, Catal. Today 93–95 (2004) 205.
[28] A.M. Chen, H.L. Xu, Y.H. Yue, W.M. Hua, W. Shen, Z. Gao, J. Mol. Catal. A: Chem. 203 (2003) 299.
[29] R.S. Drago, K. Jurczyk, D.J. Singh, V. Young, Appl. Catal. B: Environ. 6 (1995) 155.
[30] J.T. Herron, Plasma Chem. Plasma Process. 21 (2001) 581.
[31] H. Kohno, A.A. Berezin, J.-S. Chang, M. Tamura, T. Yamamoto, A. Shibuya, S. Honda, IEEE Trans. Ind. Appl. 34 (1998) 953.
[32] K. Urashima, J.-S. Chang, IEEE Trans. Ind. Appl. 7 (2000) 602.
[33] S. Imamura, Y. Tsuji, Y. Miyake, T. Ito, J. Catal. 151 (1995) 279.
[34] A.A. Mirzaei, H.R. Shaterian, R.W. Joyner, M. Stockenhuber, S.H. Taylor, G.J. Hutchings, Catal. Commun. 4 (2003) 17.
[35] W. Weimin, Y. Yongnian, Z. Jiayu, Appl. Catal. A: Gen. 133 (1995) 81.
[36] E.R. Stobbe, B.A. de Boer, J.W. Geus, Catal. Today 47 (1999) 161.
[37] C.-J. Liu, G.P. Vissokov, B.W.-L. Jang, Catal. Today 72 (2002) 173.
[38] M.B. Kizling, S.G. Järås, Appl. Catal. A: Gen. 147 (1996) 1.
[39] Y.-P. Zhang, P.-S. Ma, X.-L. Zhu, C.-J. Liu, Y.-T. Shen, Catal. Commun. 5 (2004) 35.
[40] M.H. Chen, W. Chu, X.Y. Dai, X.W. Zhang, Catal. Today 89 (2004) 201.